Thermochimica Acta 523 (2011) 90–96

Contents lists available at ScienceDirect

Thermochimica Acta

journal homepage: www.elsevier.com/locate/tca

Temperature-programmed and X-ray diffractometry studies of hydrogen-reduction course and products of WO_3 powder: Influence of reduction parameters

M.I. Zaki*, N.E. Fouad, S.A.A. Mansour, A.I. Muftah

Chemistry Department, Faculty of Science, Minia University, El-Minia 61519, Egypt

ARTICLE INFO

Article history:
Received 8 October 2010
Received in revised form 30 April 2011
Accepted 4 May 2011
Available online 11 May 2011

Keywords:
Tungsten(VI) oxide
Temperature-programmed reduction
Reduction course
Reduction products
Impacts of reduction parameters
X-ray diffractometry

ABSTRACT

The hydrogen-reduction course and products of synthetic tungsten(VI) oxide (WO_3) were examined by means of temperature-programmed reduction (TPR) and X-ray powder diffractometry (XRD) studies. A set of model tungsten compounds was procured and examined similarly for reference purposes. Results obtained could help resolving two subsequent reduction stages: (i) a low-temperature stage (<1050 K) through which WO_3 is reduced to the tetravalent state (WO_2) via formation and subsequent reduction of intermediate $WO_{2.96}$, $WO_{2.9}$, $WO_{2.72}$ oxides; and (ii) a high-temperature stage (>1050 K) through which WO_2 thus produced is reduced to the metallic state (W^o) via two intermediate oxide species (tentatively, WO and W_2O–W_3O). Reduction events involved in the high-temperature stage were found to be relatively more sensitive to the reduction parameters; namely, the starting oxide mass, heating temperature and rate, and gas flow rate and composition. They were also found to require lower activation energies than those required by events occurring throughout the low-temperature stage, a fact that may suspect compliance of the high-temperature reduction events to autocatalytic effects.

© 2011 Elsevier B.V. All rights reserved.

1. Introduction

Hydrogen-reduction of tungsten(VI) oxide (WO_3) powder has been industrially favored as a feasible means of recovery of tungsten metal (W^o) particles, which enjoy a number of application-worthy properties ([1] and references therein cited). Hence, the reduction process has been the focus of numerous research investigations including extensive thermodynamic [1,2], kinetic [3–5], morphological [1,6,7], and characterization [1,8–12] studies. These studies employed a wide range of bulk and surface, isothermal and nonisothermal, thermoanalytical (TGR, TPR, TPO and TPD), microscopic (TEM and SEM) and spectroscopic (XRD, IR, Raman, XPS, etc.) methods. A thorough inspection of the results reveals a complex nature for the reduction events, pathways and products of the oxide.

Being a solid state reaction occurring at gas/solid interfaces, the overall reduction process ($WO_{3(s)} + 3H_{2(g)} = W^o{}_{(s)} + 3H_2O_{(g)}$) has been suggested [13] to commence via adsorptive interactions of H_2 molecules with the WO_3 particles. XPS examination [13] disclosed that W^{5+} ions are initially formed on the surface due to conversion of one of the oxide oxygen ligands into OH-groups as a result of dissociative chemisorption of H_2. Upon further reduction, oxygen vacancies are progressively formed and, hence, W^{4+} ions are generated and paired with the metallic state (W^o) to show an apparent oxidation state of “2+”. These reductive modifications of the surface chemistry of WO_3 particles have been, a few years later, allocated the responsibility of alkene and alkane reforming catalytic activity shown to develop with time of thermal treatment of the oxide particles in H_2 atmosphere [14–17]. Precisely speaking, it is the pertinent population of density of states in the 5d and 6s orbitals [1] that develops the metallic character required for the initial hydrogenation/dehydrogenation of the hydrocarbon; whereas, the generated OH-groups provide the necessary Brönsted acidity for the subsequent skeletal rearrangement (isomerization) [18]. Further development of the metallic character pertaining to deepening of the reduction into the metallic (W^o) state would then trigger the undesirable hydrogenolysis of the hydrocarbon reformation products [18].

Incursion of the reduction interface (i.e., reaction front) into the bulk of the oxide particles has been found to yield a number of thermodynamically feasible intermediate oxide compositions underway to formation of the tungsten metal (W^o) particles [1]. Reportedly [1–12], oxides having compositions like $WO_{2.96}$, $WO_{2.9}$, $WO_{2.72}$, WO_2, WO, and W_3O may be formed. Temperature, kinetics, pathway and sequence of formation of these intermediate oxides have been suggested to be critically controlled by the H_2-reduction

---

* Corresponding author. Tel.: +20 102217470; fax: +20 862360833.
E-mail address: mizaki@link.net (M.I. Zaki).

0040-6031/$ – see front matter © 2011 Elsevier B.V. All rights reserved.
doi:10.1016/j.tca.2011.05.004

parameters (heating rate, gas flow rate, etc.) [1]. A shortcut to the nucleation of W^o species during early stages of WO_3 reduction is likely, but under specific reduction conditions [1,4,5]. Such an early generation of W^o nuclei has been found to evolve autocatalysis in the reduction course [4,5]. The known hydrogen dissociative activity of W^o sites [1], and consequent spillover of the hydrogen atoms thus generated [19] onto the underlying WO_3 species, catalytically enhance their further reduction to the metallic state [4,5]. Atomic hydrogen has, also, been found [20,21] to interact with WO_3 particles near ambient conditions leading to formation of hydrogen tungsten bronze (H_xWO_3, with $x \leq 0.5$).

It is worth noting, that volatile tungsten oxide hydrate ($WO_2(OH)_2$) is formed during the H_2-reduction course of WO_3 by reaction of the oxide with water that forms during the reduction [1,22,23]. $WO_2(OH)_2$ partial pressures are built up above unstable reduction products (e.g., WO_2) than above stable ones (e.g., W_3O and W^o). The pressure imbalance thus established has been suggested [1] to drive a chemical vapor transport (CVT) of tungsten, which finally leads to a dissolution (oxidation) of unstable products ($WO_2 \rightarrow WO_2(OH)_2$) and the growth of stable ones through deposition of tungsten metal via decomposition (reduction) of $WO_2(OH)_2$. This CVT process, which is considered a fascinating peculiarity of the W–O–H reduction system [1], has been found to critically control particle morphological characteristics of WO_3 reduction products [6,7].

Overall, it has been emphasized [1] that a meaningful comparison between results of reduction studies of metal oxides, performed in various laboratories, demands obtaining the results under identical processing parameters. Therefore, the present investigation was designed to examine influence of reduction parameters (namely, starting oxide mass, heating temperature and rate, and gas composition and flow rate) on the hydrogen-reduction events, course and products of finely-divided WO_3 particles. To accomplish this objective, (i) reduction events occurring throughout the reduction course (up to 1373 K) have been monitored in nonisothermal and isothermal temperature-programmed reduction (TPR) profiles measured as a function of the processing parameters concerned, (ii) TPR profiles have been deconvoluted and quantified in order to facilitate reduction stoichiometry calculations, (iii) not only synthetic WO_3, but also model (commercial) WO_3, $WO_{2.9}$, WO_2 and W^o powders were subjected to TPR analysis in order to help assigning the reduction events observed to specific reduction steps and products, and (iv) crystalline phase composition of isothermal reduction products has been identified by X-ray powder diffractometry (XRD).

It is worth noting, that the above shown breadth of test process variables and materials, as well as the diverse measurement modes (isothermal and nonisothermal mode), are not encounterable in a single relevant investigation of those previously reported and herein cited. This is meant, foremost, to bridge existing gaps of knowledge regarding the present subject matter, and provide quantitative basis for assignments to be made for reduction events and products resolved by deconvolution of the TPR profiles.

2. Experimental

2.1. Materials

Powders of model (commercial) tungsten metal (W^o) and oxides (WO_3, $WO_{2.9}$ and WO_2) were ≥99% pure products of BDH. They are discerned throughout the text by suffixing (M), for model, to the respective molecular formula. Powder of synthetic tungsten(VI) oxide (denoted WO_3(S)) was obtained by calcination of ammonium paratungstate particles ($(NH_4)_{10}[H_2W_{12}O_{42}]$; >99% pure product of Fluka Chemie) at 773 K for 10 h in a still atmosphere of air according to Fouad et al. [24]. Prior to application, test powders were ground to an average particle size <200 μm. H_2 and N_2 gases were 99% pure products of Egyptian Company of Industrial Gases (El-Hawamddyia/Egypt). They were used as supplied.

2.2. Temperature-programmed reduction (TPR)

TPR profiles were automatically measured during heating test samples (mass = 5–350 mg) at various temperature ramping rates (5–20 K/min), using a ChemBET 3000 (Quantachrome/USA). Measurements were carried out in nonisothermal mode up to 1373 K, or isothermal mode at various temperatures (873–1273 K) for 60 min, under a streaming gas mixture of 5% (or 50%) H_2/N_2 of varied flow rates (20–80 cm^3/min). Only in the isothermal mode, the hydrogen supply was turned off during initial heating to the set temperature. Then, it was turned on at the set temperature and maintained so throughout the run duration (60 min). TPR profiles were deconvoluted using standard PeakFit software, and areas (in cm^2) of peaks thus resolved were determined and used to calculate corresponding hydrogen consumption (μmol/mol of oxide) on the basis of a predetermined calibration constant (μmol/cm^2). The calibration constant was determined from a TPR profile encompassing the complete reduction course ($WO_3 \rightarrow W^o$) of a precisely weighted amount of WO_3(M); see Fig. 3.

Activation energy (ΔE/kJ/mol) for each of the reduction steps resolved (in Fig. 3) was calculated from shifts conceded by TPR peak temperature (T_p/K) as a result of changing of the heating rate (β/K s^{-1}), implementing the following linear relationship [25]:

$$\ln\left(\frac{\beta}{T_p^2}\right) = -\frac{\Delta E}{RT_p} + \ln\left(\frac{AR}{\Delta E}\right) \tag{1}$$

where A is the frequency factor and R is the universal gas constant. Thus, the activation energy was derived from slope of plots of $\ln(\beta/T_p^2)$ versus $(1/T_p)$.

2.3. X-ray powder diffractometry (XRD)

XRD analysis of test samples was performed by means of a model JSX-60PA Jeol diffractometer (Japan) equipped with Ni-filtered CuKα radiation (0.15418 nm, 40 kV and 30 mA). The data were acquired stepwise (2°/s) in the 2θ range 5–100° with a divergence slit of 2°. For identification purposes of crystalline phase composition, diffraction patterns obtained were matched with standard diffraction data (JCPDS) files [26].

3. Results and discussion

3.1. Reduction course and products

3.1.1. Nonisothermal reduction

Nonisothermal TPR profiles obtained in a hydrogen-poor atmosphere (5% H_2/N_2) for the model oxides WO_2(M), $WO_{2.9}$(M) and WO_3(M) are compared in Fig. 1 (a–c, respectively). A TPR profile obtained only for WO_3(M) in a hydrogen-rich atmosphere (50% H_2/N_2) is also included in Fig. 1(d). Profile-(a) indicates that reduction of WO_2(M) does not commence detectably unless the temperature exceeds 1200 K. The corresponding reduction event is shown not to reach its peak even at 1400 K. Hence, the shoulder and peak monitored in profile-(b) at 1066 and 1210 K, respectively, may account for a two-step reduction of $WO_{2.9}$(M) to WO_2, whose reduction is shown to commence at the immediate vicinity of its formation. Similar two reduction events, manifested by two well resolved peaks at 1066 and 1140 K, are shown to be preceded by an ill-defined shoulder (at 969 K) in profile-(c) obtained for WO_3(M) (Fig. 1). This shoulder, which is not monitored in profile-(b), may be plausibly assigned for reduction of $WO_3 \rightarrow WO_{2.9}$. Hence, the

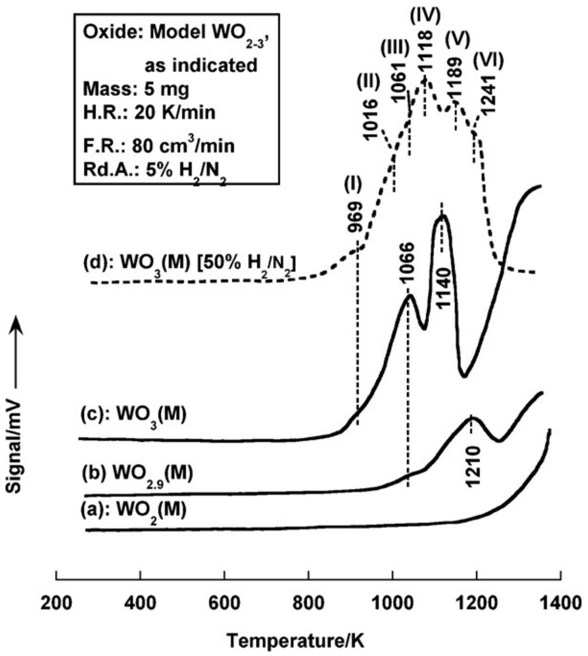

Fig. 1. TPR profiles obtained for the indicated model tungsten oxides ($WO_{2\text{–}3}$(M)), under the inset invariant conditions: oxide mass, heating rate (H.R.), gas flow rate (F.R.), and composition of reduction atmosphere (Rd.A.). The dashed profile (d) was obtained for WO_3(M) at similar conditions, but in the hydrogen-richer atmosphere of 50% H_2/N_2.

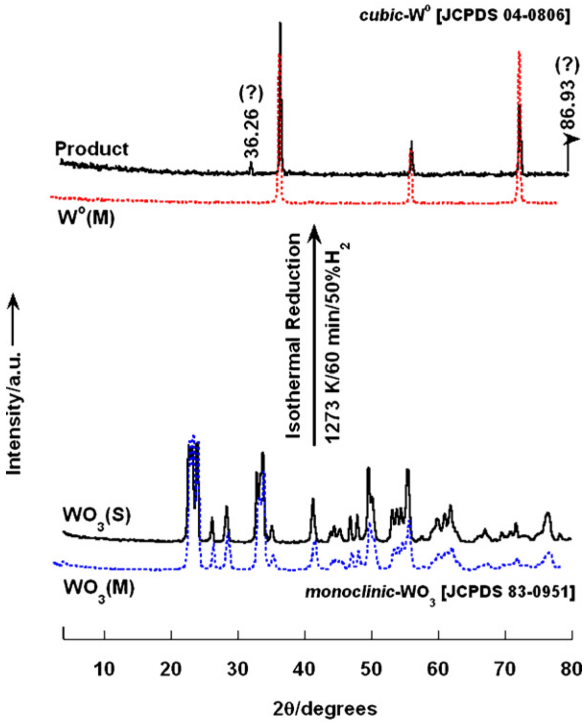

Fig. 2. X-ray powder diffractograms obtained for WO_3(S) and its isothermal reduction product under the conditions specified. Diffractograms obtained for model WO_3(M) and W^o(M) are inset for comparison purposes.

succeeding two peaks are most likely those related to reduction of the product $WO_{2.9} \rightarrow WO_2$, whereas reduction of WO_2 thus produced might be that responsible for the following incomplete peak commencing near 1200 K.

When reduction of WO_3(M) was carried out in the hydrogen-rich atmosphere of 50% H_2, the obtained TPR profile (d, Fig. 1) displays a very broad, composite peak extending over the temperature range of 800–1273 K. It is shown to resolve 6 maxima: I at 969 K, II at 1016 K, III at 1061 K, IV at 1118 K, V at 1189 K, and VI at 1241 K. An analogous sort of experiment was carried out on WO_3(S) (i.e., synthetic WO_3) in pure (100%) H_2 atmosphere. The sample mass was watched thermogravimetrically, and results obtained (Fig. S1; Supporting Information File) helped determining a total mass loss of 21.8% at 1073 K. When the gas atmosphere was changed into pure N_2, the thermogram obtained (Fig. S1) on heating up to 1373 K revealed high thermal stability for WO_3(S). This result proves that the mass loss affected in the H_2 atmosphere is due to thermochemical reduction rather than thermal decomposition. Fig. S1 shows, furthermore, that the total mass loss determined (21.8%), which would then correspond to quantitative reduction of $WO_3 \rightarrow W^o$ (20.7% expected), is made up in three cumulative mass loss steps: 1.7% at 800–873 K, 7.3% at 873–923 K, and 21.8% at 1020–1100 K. Molecular stoichiometry calculations help attributing the first mass loss step (1.7%) to reduction of $WO_3 \rightarrow WO_{2.72}$ (1.9% expected), the second (7.3%) to further reduction to WO_2 (6.9% expected), whereas the third step (21.8%) to the reduction to the metallic state (20.7% expected).

In order to identify nature of the final reduction product, a similar TPR experiment was performed on a sample of WO_3(S) but under isothermal conditions (at 1273 K for 60 min). Both of the starting oxide and the final product were then subjected to XRD analysis. The powder diffractogram obtained for WO_3(S) is shown (Fig. 2) to be very similar to that obtained for the corresponding model oxide (WO_3(M)) in identifying a sole crystalline phase having the composition of monoclinic-WO_3. On the other hand, the final reduction product is found to give rise to a diffraction pattern quite matching that obtained for model W^o metal (cubic-W^o, Fig. 2), which is the same crystalline phase composition assumed by the so-called α-W^o [1,10].

Accordingly, the composite reduction peak (at 800–1273 K) monitored in the TPR profile of WO_3(M) under the H_2-rich atmosphere (profile (d), Fig. 1) is proven to encompass a complete reduction course, i.e., $WO_3 \rightarrow W^o$. The fine structure of the peak may thus account for a complex course of reduction. As a matter of fact, the 6 reduction steps resolved and their corresponding positions at the temperature scale (I–VI) were determined in the light of the deconvolution results demonstrated in Fig. 3. Based on the amount of the starting oxide used (5-mg WO_3), the integrated (total) area of the composite peak (=126.33 cm^2) and area of each of the resolved 6 peaks, amounts of hydrogen consumed in the various reduction steps resolved were determined and set out in Table 1. These

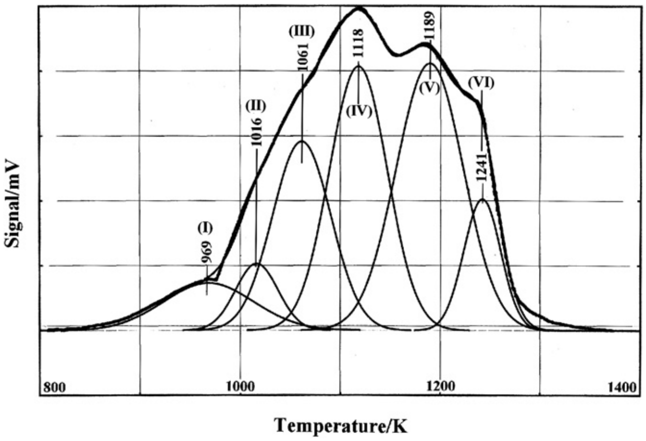

Fig. 3. Deconvoluted TPR profile obtained for reduction of WO_3(M) in the hydrogen-rich gas atmosphere (50% H_2/N_2) (profile (d) in Fig. 1).

Table 1
Hydrogen consumption as derived from areas of peaks resolved in the deconvoluted TPR profile (Fig. 3) for the complete reduction of WO_3 to W^o.

Peak number[a]	T_{max}[a] (K)	Area (cm^2)	H_2 consumption[b] (μmol)	H_2 consumption[(cum)c]		Expected reduction[d]	
				(μmol)	(%)	Product	(%)
I	969	5.05	2.587	2.587	4.0	$WO_{2.9}$	3.7
II	1016	6.70	3.430	6.017	9.3	$WO_{2.7}$	8.3
III	1061	30.20	15.462	21.479	33.2	WO_2	33.3
IV	1118	39.93	20.444	41.923	64.8	WO	66.7
V	1189	26.62	13.631	55.559	85.9	$\left\{ \begin{array}{c} W_2O– \\ W_3O \end{array} \right\}$[e]	$\left\{ \begin{array}{c} 83.3– \\ 88.9 \end{array} \right\}$
VI	1241	17.83	9.134	64.693	99.9	W^o	100.0
Total		126.33	64.688				

[a] According to Fig. 3.

[b] Derived from each corresponding peak area implementing the calibration constant (0.512 μmol/cm^2) as determined from the sample mass (5-mg WO_3) and the integrated (total) peak area (126.33 cm^2).

[c] Cumulative H_2 consumption as derived from areas of peaks (I); (I) + (II); (I) + (II) + (III), etc.

[d] WO_3 was the starting oxide for each step.

[e] Metal-rich species, where W_3O has been indexed as β-W^o [1].

data could help calculating the cumulative hydrogen consumption listed (in μmol and %), on the basis of which expected reduction products and percentages are also given alongside in Table 1. It is obvious from these results that values of % cumulative hydrogen consumption are satisfactorily close to % reduction values expected to accompany a stepwise reduction of $WO_3 \rightarrow WO_{2.9}$ (3.7%; 969 K), $WO_{2.72}$ (8.3%; 1016 K), WO_2 (33.3%; 1061 K), WO (66.7%; 1118 K), W_2O–W_3O (83.3–88.9%; 1189 K) and W^o (100%; 1241 K). Accordingly, the TPR deconvolution results (Fig. 3 and Table 1) do not account for WO_3 reduction to $WO_{2.96}$ that has been reported [6] to be the initial step in the oxide reduction course.

Several literature reports [1,10,11] have also suggested formation of the suboxides $WO_{2.9}$ and $WO_{2.7}$ during the reduction of $WO_3 \rightarrow WO_2$. Formation of these suboxides is thermodynamically sustained [2,27], and should be preceded by formation of $WO_{2.96}$ as the earliest reduction product of WO_3 [6]. In contrast, formation of the suboxide WO in the course of reduction of WO_2 to the metallic state (W^o) has only infrequently reported [1]. Whereas, tungsten-rich oxides (W_nO, where $n \geq 2$) with obvious metallic character, have been encountered and reported previously [1]. Namely, W_3O has been observed repeatedly in the reduction course not only of WO_2, but also of $WO_{2.9}$, and denoted β-W^o [1,12].

3.1.2. Isothermal reduction

Fig. 4 compares TPR profiles obtained isothermally for WO_3(S) at each of the indicated temperatures (873–1273 K) for 60 min. The test sample was firstly heated at 20 K/min up to the set temperature in pure N_2 atmosphere. Then, the gas atmosphere was switched to 5% H_2/N_2 and the measurements started. At 873 K, the profile monitors an early sharp peak after the elapse of 167 s, which is shown to be maintained occurring at the same speed in the other high-temperature profiles (973–1273 K). This peak is followed by two weak maxima at 833 and 1487 s, which are shown to be speeded up and merge into a single maximum with temperature increase. A third maximum is shown to emerge at 2282 s in the profile obtained at 973 K. It is also speeded up with temperature to occur after the elapse of 1730 s at 1073 K, and 1423 s at 1273 K. At 1073 K, the profile monitors an indication of the occurrence of a slow reduction event (at >2500 s) that seems not to be enhanced significantly at the higher temperature of 1273 K. Similar isothermal reduction events have been encountered previously by Wilken et al. [6] and Venables and Brown [11]. The initial, sharp peak was attributed by the former authors to formation of $WO_{2.96}$, and by the latter authors [11] to formation of WO_2. Hence, the subsequent events were thought by the former authors [6] to account for a stepwise ($WO_{2.96} \rightarrow WO_{2.72} \rightarrow WO_2$) reduction to the metallic state (W^o), whereas the latter authors [11] ascribed subsequent events to WO_2 reduction to W^o. It is worth mentioning, that the results of Wilken et al. [6] were obtained by following changes in the dew point of the gas atmosphere, whereas those of Venables and Brown [11] were obtained by TCD tracing. Thus, the two studies employed two different experimental methods, which are yet different from the method applied in the present study.

Therefore, the 1-h isothermal reduction product at each of the reduction temperatures adopted (Fig. 4) was subjected to XRD analysis and diffractograms thus obtained are exhibited in Fig. 5. Also exhibited in Fig. 5 are diffractograms given rise by the model oxides WO_3(M), $WO_{2.9}$(M) and WO_2(M), for comparison purposes. It is obvious from Fig. 5 that a great deal of the diffraction peaks observed for the reduction product of WO_3(S) at 873 K (for 60 min) owe their existence to the starting oxide, whereas the rest are shown to be assignable to monoclinic-$WO_{2.9}$ [JCPDS 73-2182]. This result may sustain an earlier suggestion [1] ascribing the fastest reduction event observed (the 167-s peak, Fig. 4) to H_2-uptake and

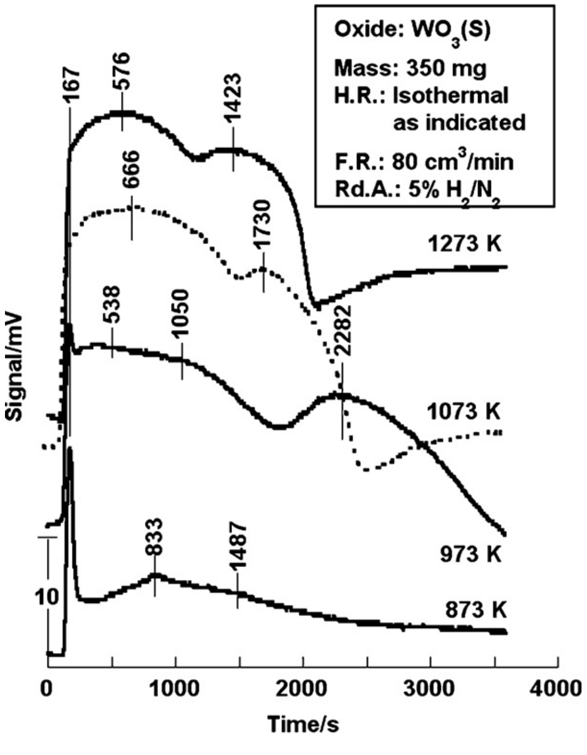

Fig. 4. Isothermal TPR profiles obtained for WO_3(S) being heated at each of the indicated temperatures (873–1273 K) for 60 min, under the conditions inset.

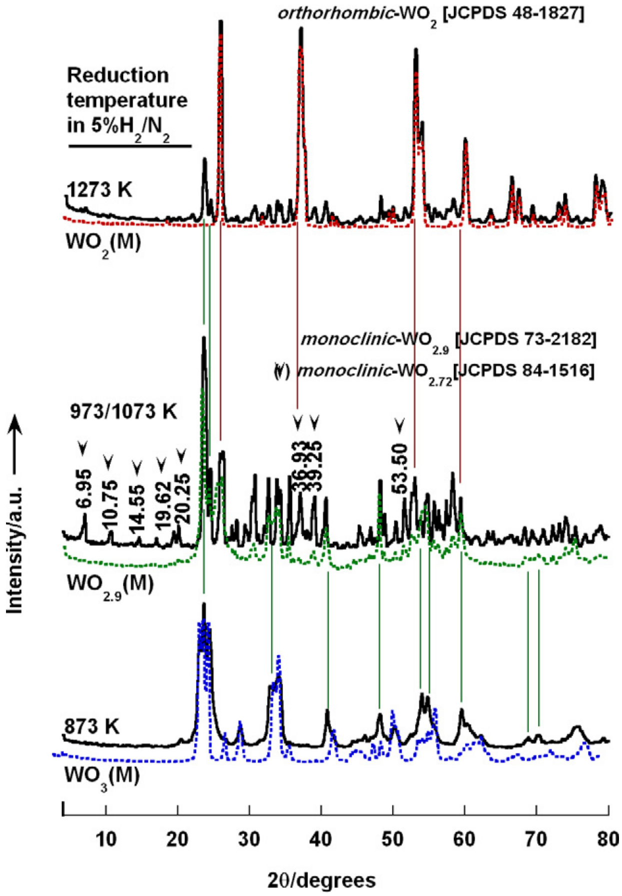

Fig. 5. X-ray powder diffractograms obtained for isothermal reduction products of WO_3(S) at each of the indicated temperatures (873–1273 K) for 60 min. Diffractograms obtained for model oxides WO_3(M), $WO_{2.9}$(M) and WO_2(M) are inset for comparison purposes.

reduction of WO_3 into $WO_{2.96}$, whereas the subsequent peak at 833 s to a further reduction of the product $WO_{2.96}$ to give $WO_{2.9}$. Formation of $WO_{2.96}$ has been considered [6] to follow formation and subsequent decomposition of tungsten bonze (H_xWO_3) [20,21]. The shoulder emerging a bit later (at 1487 s) in the TPR obtained at 873 K (Fig. 4) may be tentatively related to a much slower event (at this temperature) which does not lead to an XRD-detectable product.

Diffractograms obtained for the isothermal reduction products of WO_3(S) at 973 and 1073 K were rather similar in identifying $WO_{2.9}$ as the major crystalline phase (Fig. 5). Some other (weak) peaks that are not related to the $WO_{2.9}$ (Fig. 5), are displayed and found to account for monoclinic-$WO_{2.72}$ (JCPDS 84-1516]. As is shown in Fig. 4, isothermal reduction events assignable to formation at 873 K of $WO_{2.9}$ (peak at 833 s) and $WO_{2.72}$ (peak at 1487 s) are expedited to occur after the elapse of 538 and 1050 s, respectively, upon increasing the temperature up to 973 K. Upon further increase of the temperature up to 1073 K the two peaks (particularly that due, suggestively, to formation of $WO_{2.72}$) converge in one broad peak maximized at 666 s. The peak emerging at 2282 s in the profile obtained at 973 K, which is also enhanced to occur at 1730 s upon increasing the temperature up to 1073 K, is shown to be followed by a slight consumption of hydrogen (at ≥2400 s) at 1073 K. Reduction product(s) of these latter events seem to have not been developed into XRD-detectable crystalline phase(s).

Isothermal reduction product at 1273 K is shown by XRD to consist of a major crystalline phase exhibiting a diffraction pattern very similar to that feild (JCPDS 48-1827) for orthorhombic-WO_2 (Fig. 5). A few residual, weak peaks that do not relate to the WO_2 phase are comparable to small proportions of unreduced $WO_{2.9}$ and $WO_{2.72}$ (Fig. 5). With reference to the standard data filed in JCPDS 04-0806 (Fig. 2), coexistence of minority crystallites of W^o cannot be excluded with certainty. Accordingly, the further enhanced isothermal reduction events maximized at 576 and 1423 s in the TPR profile measured for WO_3(S) at 1273 K (Fig. 4) evidently encompass the formation of $WO_{2.9}$, $WO_{2.7}$ and WO_2 as intermediate products in the reduction course of the trioxide to the metallic state. The sharp peak at 167 s may, according to literature reports [1], be considered indicative for the formation of $WO_{2.96}$ as the initial reduction product. The rapidity and expected minute consumption of H_2 responsible for the reduction of WO_3 into $WO_{2.96}$ may explain whey it went unnoticed in the corresponding nonisothermal TPR profiles (c and d, Fig. 1). The slow event appearing at ≥2000 s (Fig. 4) is presumably corresponding to WO_2 reduction to W^o via formation and subsequent reduction of WO and W_2O–W_3O. It is worth noting, that compositions of the intermediates WO and W_2O–W_3O are suggested solely on basis of TPR deconvolution results (Fig. 3 and Table 1).

The increase of rate of the isothermal reduction events attributable to the reduction of $WO_{2.96}$ to $WO_{2.9}$, $WO_{2.72}$, WO_2, WO, W_2O–W_3O and W^o with temperature is often ascribed to enhanced kinetics of solid state reactions involved [1]. In previous investigations performed in this laboratory [4,5], however, experimental evidences were brought about for the involvement of autocatalysis in the hydrogen reduction course of WO_3. Genesis of a few nuclei of metallic tungsten has been considered [4,5] sufficient to affect dissociative chemisorptions of H_2 and consequent spillover of active hydrogen atoms to catalyze further reduction of unreduced oxides. Hence, involvement of autocatalysis in the present isothermal reduction experiments (Fig. 4), particularly at ≥973 K, cannot be excluded with certainty.

3.2. *Influence of reduction parameters*

Considering the conceptual reduction equation $WO_{3(s)} + 3H_{2(g)} = W^o_{(s)} + 3H_2O_{(g)}$, the reduction progress is controlled by the pressure ratio $P(H_2)/P(H_2O)$. This is in the sense that the higher the ratio is, the more enhanced the reduction progress [1]. Within this context, the WO_3 reduction enhancement observed in the hydrogen-rich atmosphere (50% H_2, profile-d, Fig. 1) as compared to the limited reduction progress accomplished in the hydrogen-poor atmosphere (5% H_2, profile-c, Fig. 1), should be understandable. Results obtained for the influence of other reduction parameters (viz. oxide mass, heating rate and gas flow rate) are presented and discussed below.

3.2.1. *Oxide mass*

Nonisothermal TPR profiles obtained as a function of WO_3(S) mass (2–118 mg) are compared in Fig. 6. The general trend exhibited by these profiles is the high-temperature shifts conceded by the hydrogen consumption peaks monitored upon increasing the oxide mass. Relatively speaking, however, low-temperature peaks, i.e. those corresponding to formation of the suboxides of WO_3 (viz. $WO_{2.9}$ and $WO_{2.72}$) are less influenced by the mass increase than the high-temperature peaks assignable to formation and reduction of WO_2. Though these profiles were measured in the hydrogen-poor atmosphere of 5% H_2, the reduction is shown to be advanced significantly when the starting oxide mass is decreased to less than 5 mg.

Increasing the oxide mass has been considered by many authors [1,28] to be pertained by increase of the build up of $P(H_2O)$ within the sample particles. Consequently, the $P(H_2)/P(H_2O)$ ratio is decreased and, in turn, the reduction progress is hampered. This becomes more obvious in the later stage of reduction (i.e.,

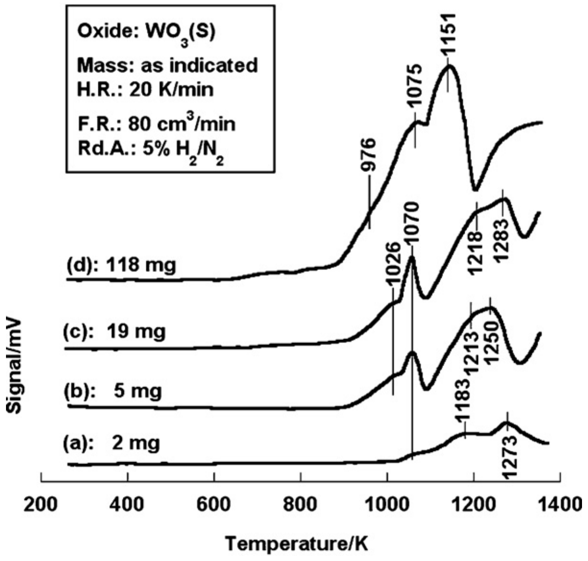

Fig. 6. TPR profiles obtained for WO_3(S) as a function of the oxide mass (2–118 mg), under the inset invariant conditions.

$WO_2 \rightarrow W^o$) because of the expected release of larger amounts of water than in the earlier stages ($WO_3 \rightarrow WO_{2.72}$). However, in the presence of only minute amounts of the oxide (<5 mg) the build up of effective water vapor pressure is not facilitated and, hence, rendered insufficient to hamper the advance of WO_3 reduction towards the metallic state. The TPR profile obtained for 2-mg WO_3 in the hydrogen-poor atmosphere of 5% H_2 (Fig. 6) is almost analogous to that obtained for 5-mg WO_3 in the hydrogen-rich atmosphere of 50% H_2 (Fig. 1).

3.2.2. Heating rate

TPR profiles obtained in 5% H_2/N_2 for WO_3(S) as a function of heating rate (5–20 K/min) are compared in Fig. 7. The results show the peak temperatures to increase with heating rate, as has often been encountered in the literature [1,28]. The four peaks monitored (I–IV) correspond to the reduction of WO_3 to $WO_{2.9}$ (I), $WO_{2.72}$ (II), WO_2 (III), and WO (IV). The hydrogen consumption monitored to follow peak-IV is indicative of commencement of the reduction of WO_2. Implementing Eq. (1) plots of $\ln(\beta/T_p^2)$ versus $(1/T_p)$ were constructed and shown in Fig. S2. Activation energy values there from derived are set out in Table 2. The activation energy values obtained for peak-I (93.4 kJ/mol) and -II (109.4 kJ/mol) are higher than those obtained for peak-III (63.7 kJ/mol) and -IV (72.7 kJ/mol). Fouad et al. [4,5] determined similar values (90–123 kcal/mol) for corresponding H_2-reduction steps of WO_3, adopting isothermal and nonisothermal gravimetry measurements. These authors have attributed [4,5] the low energy values to involvement of autocatalytic reduction due to development of nuclei of metallic tungsten. A similar reasoning has been put forward by other authors [28]. Autocatalysis has been suggested [6] to be more likely involved in the reduction course of WO_2–W^o (second stage) than in that of WO_3–WO_2 (first stage).

Table 2
The activation energy values (ΔE) derived for each of the indicated reduction events (I–IV) from nonisothermal TPR profiles obtained as a function of heating rate of WO_3 (S).

Reduction event[a]	$\Delta E/(\pm 3$ kJ/mol)
I	93
II	109
III	64
IV	73

[a] According to Fig. 7.

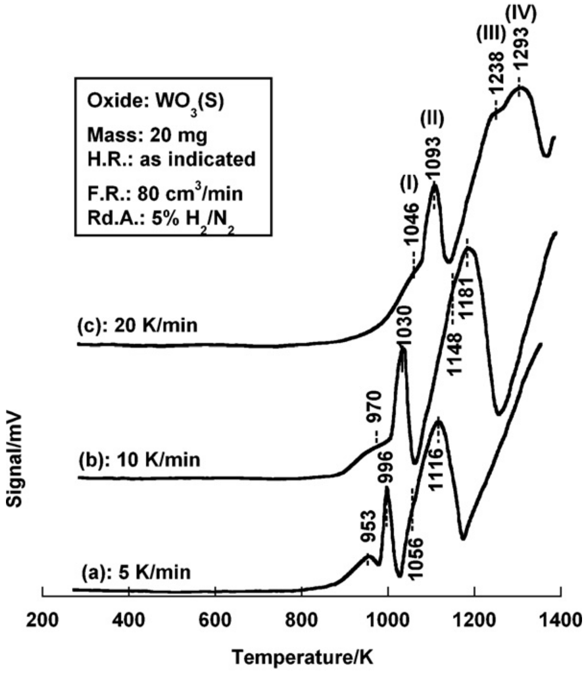

Fig. 7. TPR profiles obtained for WO_3(S) as a function of heating rate (5–20 K/min), under the inset invariant conditions. Peak designations (I–IV) are the same as in profile-d of Fig. 1.

3.2.3. Gas flow rate

TPR profiles obtained for WO_3(S) at 20 K/min as a function of the gas (5% H_2/N_2) flow rate (20–80 cm^3/min) are exhibited in Fig. 8. Results indicate that increasing the gas flow rate leads

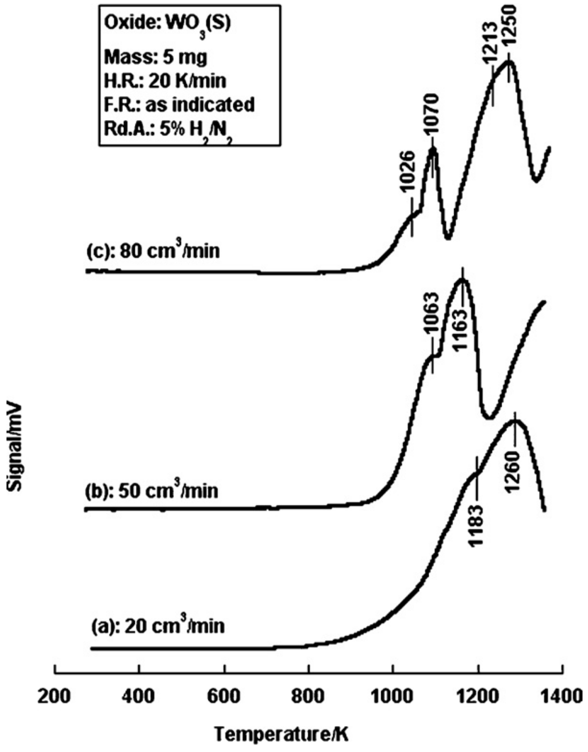

Fig. 8. TPR profiles obtained for WO_3(S) as a function of gas flow rate (20–80 cm^3/min), under the inset invariant conditions.

to decreasing peak temperatures. Accordingly, the TPR obtained under 20 cm^3/min displays only two strongly overlapping peaks at 1183 and 1260 K. These two peaks are shifted to the lower temperatures of 1063 and 1163 K, and further to 1026 and 1070 K upon increasing the gas flow rate up to 50 and 80 cm^3/min, respectively. Moreover, a third incomplete reduction peak is monitored at 50 cm^3/min. This peak, as well as a fourth one, is shown to be completed, maximizing at 1213 and 1250 K, upon increasing the gas flow rate up to 80 cm^3/min. The four peaks monitored in the TPR profile obtained at 80 cm^3/min are most probably those (I–VI) monitored in the TPR profile-c displayed in Fig. 7 and assigned, respectively, to the stepwise reduction of WO_3 to $WO_{2.9}$, $WO_{2.72}$, WO_2 and WO as in profile-d of Fig. 1. The communicated direct relationship between the gas flow rate and easiness of reduction has been attributed [1,28] to faster removal of H_2O vapor the higher the gas flow rate, thus increasing the pressure ratio $P(H_2)/P(H_2O)$. This is in the sense that accumulated water vapor (reduction product) within the oxide particles may re-oxidize the oxide thus hampering the reduction progress [1].

4. Conclusions

The above presented and discussed results may help drawing the following conclusions:

1. Two stages are discerned in the H_2-reduction course of synthetic WO_3 particles: a low-temperature stage ($WO_3 \rightarrow WO_2$ at <1050 K) involving formation and reduction of three intermediate suboxides of WO_3 (viz., $WO_{2.96}$, $WO_{2.9}$ and $WO_{2.72}$), and a high-temperature stage ($WO_2 \rightarrow W^o$ at >1050 K) involving formation and reduction of two intermediate suboxides of WO_2 (tentatively, WO and W_2O–W_3O).
2. $WO_{2.96}$ is the first reduction product of WO_3, whose formation is detectable only in isothermal TPR profiles after the elapse of 167 s (Fig. 4). The corresponding hydrogen consumption peak is most prominent in the TPR profile obtained at 873 K (Fig. 4).
3. The high-temperature stage of WO_3 reduction ($WO_2 \rightarrow W^o$) is more facile (ΔE = 63.7–72.7 kJ/mol) than the low-temperature stage (ΔE = 93.4–109.4 kJ/mol), most probably due to contribution of autocatalytic reduction associated with early nucleation of metallic tungsten species (the metal or metal-rich oxides).
4. Reduction of WO_3 is enhanced upon increasing the $P(H_2)/P(H_2O)$ pressure ratio, with the hydrogen pressure being more influential in the low-temperature stage, and the water vapor pressure is likewise but in the high-temperature stage. This can be accomplished by increasing amount of hydrogen in the gas atmosphere, or decreasing amount of the starting oxide (WO_3) and/or increasing the gas flow rate. The specified changes of the latter two reduction parameters are reflected in decreasing the build up of water vapor pressure within the oxide particles.
5. A justifiable comparison of reported reduction results of WO_3 is established only on grounds of identical (or very close) reduction parameters (heating rate, gas composition, oxide mass and gas flow rate).

Acknowledgement

The authors are indebted to the Alexander von Humboldt-Foundation (Bonn) for an equipment donation (V-815/03029). AIM appreciates a financial support from Minia University Research Administration.

Appendix A. Supplementary data

Supplementary data associated with this article can be found, in the online version, at doi:10.1016/j.tca.2011.05.004.

References

[1] E. Lassner, W.-D. Schbert, Tungsten Properties, Chemistry, Technology of the Element, Alloys and Chemical Compounds, Kluwer Academic/Plenum Publishers, New York, 1999.

[2] L. Sha, Z.J. Qiu, Thermodynamic calculation on reduction of tungsten oxide in H_2 atmosphere, Int. J. Refract. Met. Hard Mater. 26 (2008) 362–366.

[3] J.A. Bustnes, D. Sichen, S. Seetharaman, Application of a nonisothermal thermogravimetric method to the kinetic study of the reduction of metallic oxides. Part II. A theoretical treatment of powder bed reduction and its application to the reduction of tungsten oxide by hydrogen, Metall. Trans. B 24 (1993) 475–480.

[4] N.E. Fouad, Impacts of hydrogen spillover on the reduction behavior of tungsten oxide: isothermal and non-isothermal approaches, J. Anal. Appl. Pyrol. 44 (1997) 13–28.

[5] N.E. Fouad, K.M.E. Attyia, M.I. Zaki, Thermogravimetry of WO_3 reduction in hydrogen: kinetic characterization of autocatalytic effects, Powder Technol. 74 (1993) 31–37.

[6] T.R. Wilken, W.R. Morcom, C.A. Wert, J.B. Woodhouse, Reduction of tungsten oxide to tungsten metal, Metall. Trans. B 7 (1976) 589–597.

[7] V.K. Sarin, Morphological changes occurring during reduction of WO_3, J. Mater. Sci. 10 (1975) 593–598.

[8] M.G. Charlton, Hydrogen reduction of tungsten oxides, Nature 169 (1952) 109–110.

[9] J.O. Hougen, R.R. Reeves, G.G. Mannlla, Reduction of tungsten oxides with hydrogen, Ind. Eng. Chem. 48 (1956) 318–320.

[10] R. Hasegawa, T. Kurosawa, T. Yagihashi, Hydrogen reduction of tungsten trioxide and ammonium para-tungstate under high pressure, J. Jpn. Inst. Met. 15 (1974) 75–82 (Engl. Transl.).

[11] D.S. Venables, M.E. Brown, Reduction of tungsten oxides with hydrogen and with hydrogen and carbon, Thermochim. Acta 285 (1996) 361–382.

[12] A. Lackner, A. Filzwieser, P. Paschen, W. Köck, On the reduction of tungsten blue oxide in a stream of hydrogen, Int. J. Refract. Met. Hard Mater. 14 (1996) 383–391.

[13] J. Haber, J. Stoch, L. Ungier, Electron spectroscopic studies of the reduction of WO_3, J. Solid State Chem. 19 (1976) 113–115.

[14] A. Katrib, F. Hemming, P. Wehrer, L. Hilaire, G. Maire, The multi-surface structure and catalytic properties of partially reduced WO_3, WO_2 and WC + O_2 or W + O_2 as characterized by XPS, J. Electron Spectrosc. Relat. Phenom. 76 (1995) 195–200.

[15] V. Logie, P. Wehrer, A. Katrib, G. Maire, Catalytic activity of bulk WO_3 for the reforming of hexanes and hexenes, J. Catal. 189 (2000) 438–448.

[16] A. Benadda, A. Katrib, J.W. Sobczak, A. Barama, Hydroisomerization of *n*-heptane and dehydration of 2-propanol on bulk and supported $WO_2(H_x)_{ac}$ on TiO_2, Appl. Catal. A 260 (2004) 175–183.

[17] H. Al-Kandari, F. Al-Kharafi, N. Al-Awadi, O.M. El-Dusouqui, A. Katrib, Surface electronic structure–catalytic activity relationship of partially reduced WO_3 bulk or deposited on TiO_2, J. Electron Spectrosc. Relat. Phenom. 151 (2006) 128–134.

[18] J.H. Sinfelt, Catalytic reforming, in: G. Ertl, H. Knözinger, J. Weitkamp (Eds.), Handbook of Heterogeneous Catalysis, vol. 4, Wiley-VCH, Weinheim, 1997, pp. 1939–1986.

[19] P.A. Sermon, G.C. Bond, Hydrogen spillover, Catal. Rev. 8 (1973) 211–239.

[20] P.G. Dickens, J.H. Moore, D.J. Neild, Thermochemistry of hydrogen tungsten bronze phases H_xWO_3, J. Solid State Chem. 7 (1973) 241–244.

[21] B. Gerand, M. Figlarz, Spillover of adsorbed hydrogen, in: G.M. Pajonk, S.T. Teichner, J.E. Germain (Eds.), Spillover of Adsorbed Species, Elsevier Science Publishers B.V., Amsterdam, 1983, pp. 275–283.

[22] O. Glemser, H.G. Voltz, Gasformige hydroxyde. 1. Uber gasformiges $WO_2(OH)_2$, Naturwissenschaften 43 (1956) 33–133.

[23] O. Glemser, H. Ackermann, Gasformige hydroxyde. 6. Erganzende untersuchungen uber gasformige $WO_2(OH)_2$, Z. Anorg. Allg. Chem. 325 (1963) 281–286.

[24] N.E. Fouad, A.K.H. Nohman, M.I. Zaki, Spectro-thermal investigation of the decomposition intermediates developed throughout reduction of ammonium paratungstate, Thermochim. Acta 343 (2000) 139–143.

[25] J. Šesták, V. Šatava, W.W. Wendlandt, The study of heterogeneous processes by thermal analysis, Thermochim. Acta 7 (1973) 333–556.

[26] International Center for Diffraction Data, 12 Campus Boulevard, Newton Square, PA 19073-3273.

[27] Chinese Academy of Science, Basic Science Data Center, http//mole.ipe.ac.cn/all_thermochemistry/all_thermochemistry_query.aspx.

[28] P. Arnoldy, J.C.M. de Jonge, J.A. Moulijn, Temperature-programed reduction of molybdenum(VI) oxide and molybdenum(IV) oxide, J. Phys. Chem. 89 (1985) 4517–4526.